

Propargylimine in the laboratory and in space: millimetre-wave spectroscopy and first detection in the ISM

L. Bizzocchi¹, D. Prudeniano¹, V. M. Rivilla², A. Pietropolli-Charmet³, B. M. Giuliano¹, P. Caselli¹,
J. Martín-Pintado⁴, I. Jiménez-Serra⁴, S. Martín^{5,6}, M. A. Requena-Torres^{7,8}, F. Rico-Villas⁴, S. Zeng⁹, and
J.-C. Guillemin¹⁰

¹ Center for Astrochemical Studies, Max-Planck-Institut für extraterrestrische Physik, Gießenbachstraße 1, 85748 Garching (Germany) e-mail: [prudeniano,bizzocchi,giuliano,caselli]@mpe.mpg.de

² INAF-Osservatorio Astrofisico di Arcetri, Largo Enrico Fermi 5, 50125 Firenze (Italy) e-mail: rivilla@arcetri.astro.it

³ Dipartimento di Scienze Molecolari e Nanosistemi, Università Ca' Foscari Venezia, via Torino 155, 30172 Mestre (Italy) e-mail: jacpnike@unive.it

⁴ Centro de Astrobiología (CSIC-INTA), Ctra. de Torrejón a Ajalvir, km 4, Torrejón de Ardoz, 28850 Madrid (Spain)

⁵ European Southern Observatory (ESO), Alonso de Córdoba 3107, Vitacura, 763-0355 Santiago (Chile)

⁶ Joint ALMA Observatory (ESO), Alonso de Córdoba 3107, Vitacura, 763-0355 Santiago (Chile)

⁷ University of Maryland, College Park, ND 20742-2421 (USA)

⁸ Department of Physics, Astronomy and Geosciences, Towson University, Towson, MD 21252, USA

⁹ Star and Planet Formation Laboratory, Cluster for Pioneering Research, RIKEN, 2-1 Hirosawa, Wako, Saitama, 351-0198, Japan e-mail: shaoshan.zeng@riken.jp

¹⁰ Univ. Rennes, Ecole Nationale Supérieure de Chimie de Rennes, CNRS, ISCR – UMR6226, F-35000 Rennes (France) e-mail: jean-claude.guillemin@ensc-rennes.fr

June 16, 2020

ABSTRACT

Context. Small imines containing up to three carbon atoms are present in the interstellar medium. As alkynyl compounds are abundant in this medium, propargylimine (2-propyn-1-imine, $\text{HC}\equiv\text{C}-\text{CH}=\text{NH}$) thus represents a promising candidate for a new interstellar detection.

Aims. The goal of the present work is to perform a comprehensive laboratory investigation of the rotational spectrum of propargylimine in its ground vibrational state in order to obtain a highly precise set of rest-frequencies and to search it in space.

Methods. The rotational spectra of *E* and *Z* geometrical isomers of propargylimine have been recorded in laboratory in the 83–500 GHz frequency interval. The measurements have been performed using a source-modulation millimetre-wave spectrometer equipped with a pyrolysis system for the production of unstable species. High-level ab initio calculations were performed to assist the analysis and to obtain reliable estimates for an extended set of spectroscopic quantities. We have searched for propargylimine at 3 and 2 mm in the spectral survey of the quiescent giant molecular cloud G+0.693-0.027 located in the “Central Molecular Zone”, close to the Galactic Centre.

Results. About 1000 rotational transitions have been recorded for the *E*- and *Z*-propargylimine, in the laboratory. These new data have enabled the determination of a very accurate set of spectroscopic parameters including rotational, quartic and sextic centrifugal distortion constants. The improved spectral data allow us to perform a successful search for this new imine in the G+0.693-0.027 molecular cloud. Eighteen lines of *Z*-propargylimine have been detected at level $> 2.5\sigma$, resulting in a column density estimate of $N = (0.24 \pm 0.02) \times 10^{14} \text{ cm}^{-2}$. An upper limit was retrieved for the higher-energy *E* isomer, which was not detected in the data. The fractional abundance (w.r.t. H_2) derived for *Z*-propargylimine is 1.8×10^{-10} . We discuss the possible formation routes by comparing the derived abundance with those measured in the source for possible chemical precursors.

Key words. Molecular data – Methods: laboratory: molecular – Methods: observational – Techniques: spectroscopic – ISM: clouds – ISM:molecules

1. Introduction

Among the over 200 molecules detected in the Interstellar Medium (ISM) and circumstellar shells, approximately 70 have 6 or more atoms and contain carbon. In an astronomical context, these compounds are called Complex Organic Molecules (COMs, Herbst & van Dishoeck 2009), and have received an increasing attention in the last decade in an effort of unveiling how chemical complexity builds up, from simple species to the much larger molecular structures required to establish biochemical processes on planets where appropriate conditions are met. Nitrogen-bearing COMs are particularly interesting as

they can be regarded as an intermediate step towards the formation of biologically important species, such as nucleobases and amino-acids. As protein constituents, amino acids are prime targets for astrobiological studies, and their extra-terrestrial formation has been a highly debated topic. Numerous compounds of this class have been found in carbonaceous chondrites (see e.g. Cobb & Pudritz 2014, and references therein), where they are thought to form by aqueous alteration (see Burton et al. 2012 for a review on meteoritic prebiotic compounds). Glycine, the simplest amino acid, has not been detected in the ISM to date (Snyder et al. 2005), however it was found in the coma of the

67P/Churyumov–Gerasimenko comet through *in situ* mass spectrometry (Altwegg et al. 2016). The presence of glycine in the volatile cometary material thus strongly suggests the existence of a process capable to generate amino acids in cold environments and likely in absence of liquid water.

Many theoretical and laboratory studies have been devoted to the investigation of the chemical routes which may lead to amino acids in diverse extra-terrestrial environments (see e.g. Woon 2002; Koch et al. 2008; Aponte et al. 2017, and references therein). The most promising pathways in interstellar ice analogues involve, as the last step, the hydration of an aminonitrile compound ($\text{H}_2\text{N}-\text{CHR}-\text{CN}$). In astrophysical-like conditions, these precursors may be generated photochemically, i.e. through addition of ammonia to the corresponding nitrile (Danger et al. 2011b), or via the Strecker mechanism which starts from the condensation of ammonia with an aldehyde ($\text{R}-\text{CHO}$, see Danger et al. 2011a, and references therein). This latter process involves a species containing the iminic moiety ($\text{RC}=\text{NH}$) as reactive intermediate (Aponte et al. 2017).

Imines are a class of molecules that are well represented in the ISM with six members detected to date. Four are simple chains: methanimine (CH_2NH , Godfrey et al. 1973; Dickens et al. 1997), ethanimine (CH_3CHNH , Loomis et al. 2013), ketenimine (CH_2CNH , Lovas et al. 2006), and 3-imino-1,2-propadienylidene (CCCNH , Kawaguchi et al. 1992); but there are also the substituted *C*-cyanomethanimine (NCCHNH , Zaleski et al. 2013; Rivilla et al. 2019), and the cumulated “dimine” carbodiimide (HNCNH , McGuire et al. 2012). Hypotheses on their formation in astrophysical environments point mainly to a chemical route from simple nitriles via tautomerisation (Lovas et al. 2006) or by partial hydrogenation on dust grain surface (Theule et al. 2011; Krim et al. 2019).

According to this scheme, it results that, among the 3C-atom bearing imines, a new, promising candidate for the detection in the ISM would be propargylimine (2-propyn-1-imine, $\text{HC}\equiv\text{C}-\text{CH}=\text{NH}$, hereafter PGIM). This species is a structural isomer of the well-known astrophysical molecule acrylonitrile (Gardner & Winnewisser 1970) and can be chemically related — through 2H addition — to cyanoacetylene (HC_3N), a nitrile species which is ubiquitous in the ISM (e.g. Bizzocchi et al. 2017b, and references therein). Despite this, PGIM has not attracted a great deal of interest from laboratory spectroscopists and only a few, rather outdated works, are present in the literature. Its rotational spectrum was first observed in 1984 by Kroto et al. in the centimetre-wave (cm-wave) spectral region. Shortly after, the study was extended by Sugie et al. (1985) and by McNaughton et al. (1988), who also recorded a few rotational transitions for several isotopic variants. In the mid ‘80s, the observation of its low-resolution infrared (IR) spectrum was also reported (Hamada et al. 1984; Osman et al. 1987). These few laboratory studies do not provide an exhaustive spectroscopic knowledge. In particular, the coverage of the rotational spectrum is sparse and limited to the cm-wave regime, thus the reliability of the rest-frequency computed at millimetre (mm) wavelengths is not suitable for the purpose of an effective astronomical search. With this in mind, we have undertaken a new extensive laboratory investigation, recording the mm spectrum of PGIM in its vibrational ground state. The newly obtained laboratory data have been then used as a guidance to search for PGIM towards the quiescent molecular clouds G+0.693-0.027, located in the “Central Molecular Zone” in the inner ~ 500 pc of our Galaxy, where several species directly related with prebiotic chemistry have been recently detected (Requena-Torres et al. 2006, 2008; Zeng et al. 2018; Jiménez-Serra et al. 2020).

The structure of the paper is the following. In Sect. 2 we describe the experimental procedure and in Sect. 3 we provide a short account of the theoretical calculations performed to support the data analysis. Sect. 4 we describe the spectral analysis and discuss the results. In Sect. 5 we describe the observations performed to search for PGIM in the ISM and illustrate the analysis of the data which leads to its positive identification. Finally, we draw our conclusions in Sect. 6.

2. Experiments

The rotational spectrum of PGIM has been recorded using the CASAC (Center for Astrochemical Studies Absorption Cell) spectrometer at the Max-Planck-Institut für extraterrestrische Physik in Garching. Full details on the experimental set-up have been already provided (Bizzocchi et al. 2017a); here, we report only a few key details which apply to the present investigation. The instrument employs an active multiplier chain (Virginia Diodes) as a source of mm radiation in the 82–125 GHz band. This primary stage is driven by a cm-wave synthesizer which operates in the 18-28 GHz frequency range. Accurate frequency and phase stabilisation is achieved by locking the parent cm synthesizer to a Rb atomic clock. By the use of further multiplier stage in cascade, the frequency coverage can be extended towards the sub-mm regime with available power of a 2–20 μW up to 1 THz. A closed-cycle He-cooled InSb hot electron bolometer operating at 4 K (QMC) is used as a detector. The spectral measurements have been performed using the frequency modulation (FM) technique: the carrier signal from the cm-wave synthesizer is sine-wave modulated at 50 kHz and the detector output is demodulated at twice this frequency ($2f$) by a lock-in amplifier. The second derivative of the actual absorption profile is thus recorded by the computer-controlled acquisition system.

The absorption cell is a plain Pyrex tube (3 m long and 5 cm in diameter) which, at one end is connected to a side arm hosting a pyrolysis production system. This consists of a quartz tube (1 cm in diameter, 60 cm long) inserted in a tubular oven (Carbolite) which heats up the inner 40 cm long part.

PGIM was produced as in Sugie et al. (1985), i.e., by pyrolysing dipropargylamine ($(\text{HC}\equiv\text{CCH}_2)_2\text{NH}$) vapours and flowing the gaseous reaction products through the absorption cell kept under continuous pumping. In our setup, the strongest absorption signals of the target molecule were obtained by setting the oven temperature at 950°C. Typical pressure were 150–200 mTorr (20–26 Pa) at the quartz tube inlet. This corresponds to ca. 4 mTorr (0.5 Pa) in the absorption cell which was kept at room temperature. Multiple side-products are formed, as reported by McNaughton et al. (1988), which occasionally generated strong spectral features. This, however did not hamper the recording of the PGIM spectrum, thus sample purification via selective trapping or condensation/re-vaporisation were not attempted in the present investigation.

3. Molecular properties

PGIM can be described as a molecule joining two basic subunits: the ethynyl group $\text{HC}\equiv\text{C}-$ and the iminic moiety $-\text{CH}=\text{NH}$. The presence of two conjugated multiple bonds forces the molecule to the planar configuration with all the seven atoms lying on the plane defined by the *a* and *b* principal axes. Owing to different relative position of the HCC group and of the iminic H with respect to the $\text{C}=\text{N}$ double bond, two structural isomers exist: *Z* and *E*. Their structures are depicted in Fig. 1.

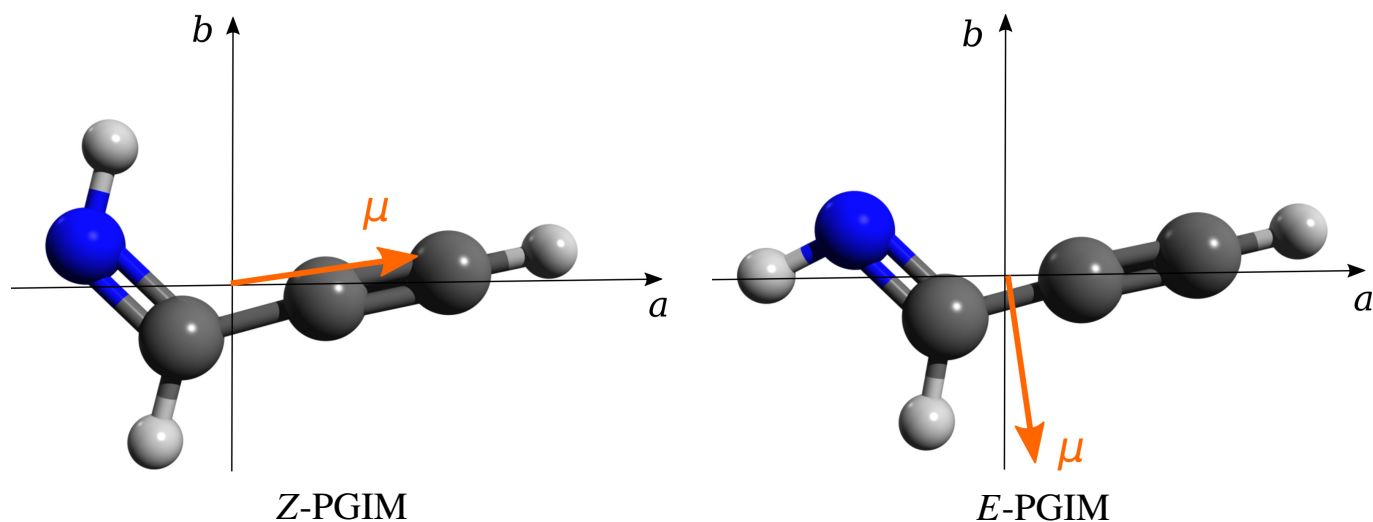


Fig. 1. Molecular structure and principal inertial axes of the *Z* and *E* isomers of PGIM. The orange arrow indicates the direction of the electric dipole moment μ and points towards the displacement of the notional negative charge. The modulus is $\mu = 2.15$ D for *Z*-PGIM and $\mu = 1.95$ D for *E*-PGIM.

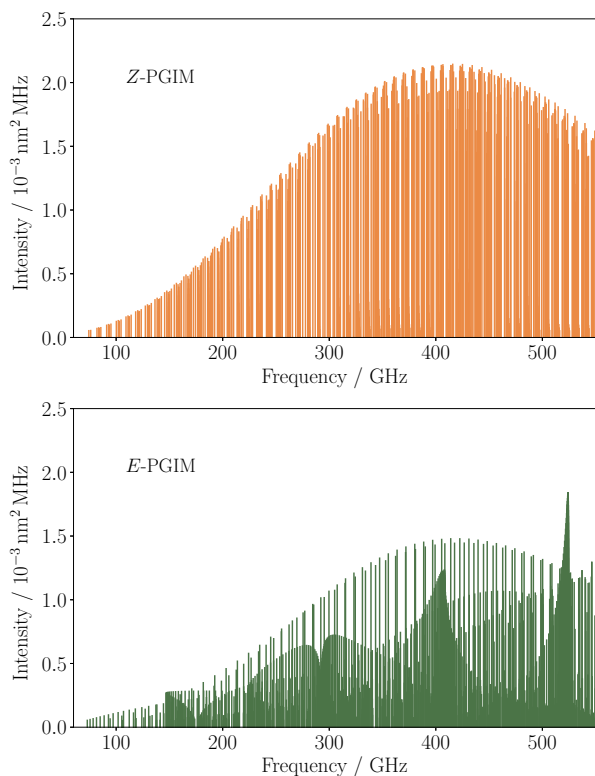


Fig. 2. Stick spectra of the *Z* (upper panel) and *E* (lower panel) isomers of PGIM computed at 300 K. Frequency positions and intensities have been computed using the spectroscopic parameters reported in Table 2 and the ab initio values of the dipole moments (see Appendix A).

With the aim of fully characterising the molecular properties of the PGIM we have conducted extensive theoretical calculations at coupled-cluster (CC) level of theory, with single and double excitations augmented by a perturbative treatment for estimating the effects of triple excitations (i.e. CCSD(T), Raghavachari et al. 1989). Appropriate extrapolation procedures to the complete basis set (CBS) limit (Heckert et al. 2005a,b) were then employed to estimate the equilibrium structures of the two conformers and their energies. Employing a similar com-

posite approach (see, for example Barone et al. 2015; Pietropoli Charmet et al. 2017a; Degli Esposti et al. 2018) the best-estimate values of the quadratic force fields were derived. Cubic and semidiagonal quartic force constants, computed at different levels of theory, were employed for the vibrational corrections to the equilibrium rotational constants, for the anharmonic corrections to the harmonic frequencies, and for determining the sextic centrifugal distortion constants. Nuclear quadrupole coupling constants for the nitrogen atoms were computed following the same procedure described previously (Cazzoli et al. 2011; Pietropoli Charmet et al. 2016). Additional details on the calculations (levels of theory, basis sets, and methodology) are reported in the Appendix A.

From our calculations the energy difference between the *Z* (more stable) and *E* isomers is $0.8510 \text{ kcal mol}^{-1}$ ($E/k = 428.2 \text{ K}$). Both isomers are prolate-type slightly asymmetric tops ($\kappa \sim 0.98$). While the modulus of the dipole moment is similar ($|\mu| \sim 2 \text{ D}$), the corresponding components in the principal axes are very different: $\mu_a = 2.14 \text{ D}$ and $\mu_b = 0.17 \text{ D}$ for the *Z* isomer; $\mu_a = 0.26 \text{ D}$ and $\mu_b = 1.93 \text{ D}$ for the *E* isomer. The dipole moment vectors are also shown in Fig. 1.

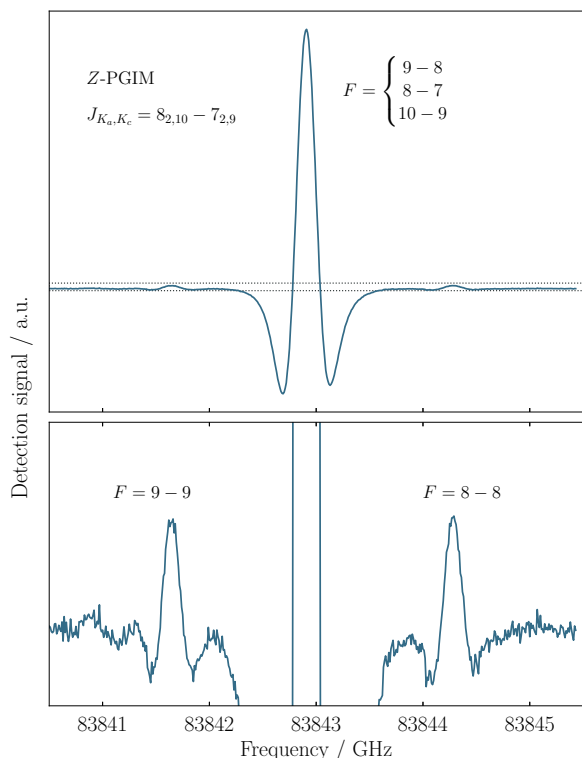
4. Spectral analysis

The rotational spectrum of PGIM has been recorded in selected frequency intervals from 83 to 500 GHz. In the mm region, *Z*-PGIM presents a typical *a*-type spectrum with groups of *R*-branch $\Delta K_a = 0$ transitions regularly separated by $\approx B + C$, (Fig. 2, upper panel), while the *E* isomer exhibits a much more complex spectrum consisting of several $\Delta K_a \pm 1$ ladders overlapped with each other and with some prominent *Q*-branch bandheads spaced by $\approx 2A - B - C$ (Fig. 2, lower panel).

From the ab initio computed energy difference, a relative $[Z]/[E]$ isomer abundance of 4.2 can be estimated at 300 K. From the relative intensity comparison between a pair of nearby *Z*- and *E*-PGIM lines recorded under the same experimental conditions (source power, sample pressure, and modulation depth) we obtained $[Z]/[E] = 4.7 \pm 0.7$, in good agreement with the theoretical computation. This indicates that, although PGIM is generated in a high-temperature environment ($\sim 950^\circ\text{C}$), there is a quick thermalisation between the two isomers, and the pop-

Table 1. Summary of the transitions with resolved hyperfine structure recorded for both PGIM isomers.

Z-PGIM				E-PGIM			
type ^a	no. of lines	no. of comp. ^b	K'_a	type ^a	no. of lines	no. of comp. ^b	K'_a
^a $R_{0,+1}$	29	76	0,1,2,3	^b $P_{+1,-1}$	10	18	1
^b $R_{+1,+1}$	4	6	0	^b $R_{0,+1}$	73	140	0,1,2
^b $R_{-1,+1}$	3	6	1	^b $Q_{+1,-1}$	50	99	0,1,2
^b $Q_{+1,-1}$	6	12	0				

^a See footnote at page 4.^b Resolved hyperfine components.**Fig. 3.** Recording of the $J_{K_a, K_c} = 8_{2,10} - 7_{2,9}$ of Z-PGIM showing the two weak $\Delta F = 0$ hyperfine components symmetrically separated from the central blended $\Delta F = +1$ triplet by 1.3 MHz (*upper panel*). Total integration time 47 s with time constant $RC = 3$ ms. The area enclosed in the dashed box is plotted with expanded y-axis in the *lower panel*.

ulation relaxes to the 300 K value right after the gas enters in contact with the cell walls.

Due to the presence of nitrogen, hyperfine coupling is generated between the molecular electric field gradient averaged over the end-over-end rotation, and the quadrupole moment of the ^{14}N nucleus having spin $I = 1$. Thus, each rotational level with principal quantum number $J > 0$ is split into three hyperfine sub-levels labelled with the total angular quantum number F , where $F = J - 1, J, J + 1$. As a consequence, the transitions are split into several components according to the $\Delta F = 0, \pm 1$ selection rules, with the strongest features being those for which $\Delta F = \Delta J$. However, in the frequency interval covered by the present investigation, the J quantum number reaches a value as high as 54,

thus most of the ^a $R_{0,+1}$ transitions¹ (which dominates the Z isomer spectrum) have their hyperfine pattern collapsed into a single feature. Nevertheless, for a few low- J lines it was possible to detect the very weak $\Delta F = 0$ components, which form a widely separated doublet approximately centred at the frequency of the corresponding unsplit transition. An example of such hyperfine patterns is given in Fig. 3. The situation is different for the *b*-type lines, typical of the *E* isomer spectrum. Due to the change in the K_a pseudo quantum number involved in these transitions, less tight hyperfine patterns are produced and triplets/doublets of lines have been generally recorded, as shown in Fig. 4. A summary of the transitions of both isomers for which the hyperfine structure have been resolved is presented in Table 1.

Whenever possible, each measured feature was assigned to a single quadrupole component. Close patterns were observed as a single line and, in this case, the intensity-averaged calculated frequency (typically of 2 or 3 components) was compared with the experimental datum in the least-squares fit. Loose blends of unresolved components have also been observed. These lines appeared as broad and distorted features and were not used in the analysis. This careful selection procedure made it possible to achieve the same measurement precision for both the singly-assigned and for the intensity-averaged hyperfine entries. A sizeable number of recorded transitions did not show any hint of hyperfine splitting, namely 381 for the Z isomer and 288 for the *E* isomer. For these data, the contributions due to the nuclear quadrupole coupling were neglected, and the measured frequencies were assigned to the corresponding pure rotational transitions. For each isomer, lines with or without resolved hyperfine structure have been given the same assumed uncertainty and have been analysed together in a global least-squares fashion.

In total, our data sets comprise 531 lines for Z-PGIM and 545 lines for *E*-PGIM. They also included 50 and, respectively, 47 cm-wave transitions taken from the literature (Sugie et al. 1985; McNaughton et al. 1988). Different statistical weights $w = 1/\sigma^2$ were given to the data of the various subsets to take into account the different measurement precision (σ). For the lines measured by Sugie et al. (1985) we retained the same weighting scheme of the original paper, while 50 kHz was given to the few transitions of the Z isomer reported by McNaughton et al. (1988). The average uncertainty of the frequencies measured in the present work is estimated to be 15 kHz. The com-

¹ The symbol ${}^x M_{\delta K_a, \delta K_c}$ is used to label in a compact form the transition type for an asymmetric rotor: x indicates the dipole moment component involved, $M = P, Q, R$ is the symbol for the transitions with $\Delta J = -1, 0, +1$, respectively, and δK_a and δK_c refer to the (signed) change of the K_a and K_c pseudo-angular quantum numbers (Gordy & Cook 1984).

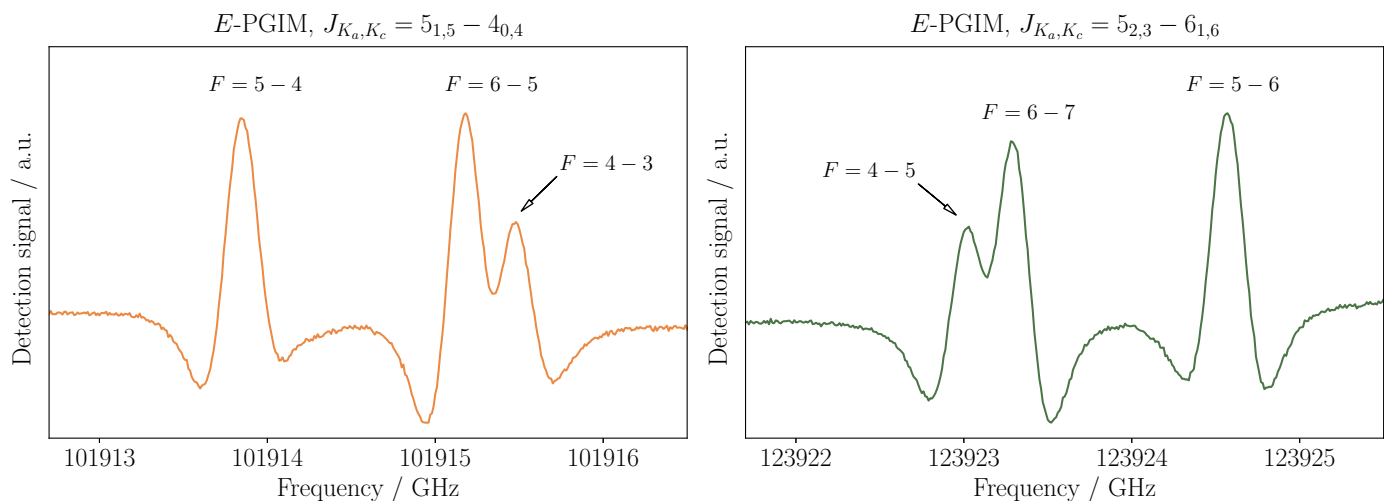


Fig. 4. Recordings of two b -type transitions for E -PGIM showing the typical hyperfine structure produced by the quadrupole coupling of the ^{14}N nucleus. *Left panel:* $J_{K_a, K_c} = 5_{1,5} - 4_{0,4}$; integration time 180 s. *Right panel:* $J_{K_a, K_c} = 5_{2,3} - 6_{1,6}$; integration time 165 s. The adopted scan rate is 0.2 MHz s^{-1} with time constant $RC = 3 \text{ ms}$.

plete data list is provided as electronic supplementary information.

The hyperfine energies were computed adopting the standard vector coupling scheme between the rotational angular momentum J and the nitrogen spin I_N :

$$\mathbf{J} + \mathbf{I}_N = \mathbf{F}. \quad (1)$$

The total Hamiltonian is thus expressed as the sum of a purely rotational part and a hyperfine contribution:

$$\hat{H} = \hat{H}_{\text{rot}} + \hat{H}_{\text{HFS}}. \quad (2)$$

The pure rotational levels are labelled with the quantum numbers J_{K_a, K_c} , the total angular momentum quantum number F must be added when the hyperfine sublevels are considered. The rotational Hamiltonian \hat{H}_{rot} is the S -reduced Watson-type Hamiltonian in its I' representation (Watson 1977) and includes centrifugal distortion corrections up to the octic terms. The hyperfine-structure Hamiltonian \hat{H}_{HFS} is expressed by the traceless tensor χ which has χ_{aa} and $\chi_{bb} - \chi_{cc}$ as determinable coefficients. This term has been considered only for the analysis of the resolved hyperfine components. The weak spin-rotation couplings of both ^{14}N and H nuclei do not produce any detectable effect in the recorded spectra and were thus neglected. All spectral computations were performed with the CALPGM suite of programs (Pickett 1991).

The spectroscopic parameters for the two propargylimine isomers are reported in Table 2 together with a compilation of theoretically computed quantities derived as described in Appendix A in the appendix. Very precise determinations of the rotational constants A, B, C were obtained, whose uncertainties are reduced by factors of 7–30 compared to the ones obtained in the previous study (Sugie et al. 1985). The quartic centrifugal distortion constants had also been determined in that work, but using an approximated perturbation expression (described in Watson 1967), so they are not directly comparable with the present results. The precision of our determined values is very high: the standard errors are generally of a few $10^{-3}\%$, only D_K for the Z isomer — for which mainly a -type transition were recorded — reaches 0.07%. A full set of sextic centrifugal distortion constants have been obtained for the first time, and their uncertainties are generally less than 1% (12% for H_K of the Z isomer). Additionally, two octic centrifugal distortion constants (L_{JK}, L_{JK}

for the Z isomer and L_{JK}, L_{JKK} for the E isomer) had to be included in the fit in order to reproduce all the measured transition frequencies within the experimental accuracy. Their values should be considered as “effective” and they are determined with 15% uncertainty at least.

The comparison between experimentally derived and theoretically computed values shows an overall excellent agreement. For the rotational constants the deviations are generally lower than 0.1%; the quartic centrifugal distortion coefficients show an average absolute deviation of less than 5% for both isomers, with only the small d_2 constants showing larger deviations. Also, the sextic centrifugal distortion constants compare well with the corresponding ab initio predictions; in all but a few cases, the deviations are within 10%. Notable exceptions are the H_K and h_3 values for the Z isomer, for which only a few b -type transitions have been recorded, thus making these parameter highly correlated with the much larger A and D_K constants.

The theoretically computed values of the quadrupole coupling tensor components are also very close to the ones derived from the experimental hyperfine structure analysis. In general, they agree within 3–4%; only χ_{aa} for the E isomer is slightly off ($\sim 10\%$), but its experimental value is also affected by a larger uncertainty and it is consistent with the ab initio prediction within 3σ .

From the spectroscopic parameters presented in Table 2 we have generated reliable sets of rest frequencies to guide astronomical searches of PGIM in the ISM. To evaluate the overall precision of our spectral computations, we have chosen a subset of transitions having $K_a = 0, 1, 2, 3$ and lower level energy, $E/k < 200 \text{ K}$. Then, we further singled out all the lines having integrated intensity of at least 1/10 of the maximum computed at 50 K. These selections constitute the most critical spectral data for an effective search of the PGIM isomers in astrophysical sources. They contain 159 lines in the 54–265 GHz range for Z -PGIM, and 247 lines in the 66–551 GHz range for the E -PGIM. The maximum 1σ errors are 1.9 kHz and 4.7 kHz, respectively, which correspond to radial equivalent velocity uncertainties in the ranges $0.8 - 2.0 \times 10^{-2}$ at 3 mm, and $0.3 - 0.8 \times 10^{-2}$ at 1 mm regime.

As electronic supplementary information, we provide a set of spectral catalogues for PGIM isomers directly obtained with the SPCAT program (Pickett 1991) without any further editing.

Table 2. Experimental and theoretical spectroscopic parameters of PGIM isomers. Numbers in parentheses are 1σ statistical uncertainties in the units of the last quoted digit.

Parameter	Z-PGIM		E-PGIM		
	exp.	ab initio ^a	exp.	ab initio ^a	
A	/ MHz	54640.1468(45)	54713.513	63099.2207(22)	63096.337
B	/ MHz	4862.362758(60)	4858.512	4766.557614(55)	4764.532
C	/ MHz	4458.249970(55)	4455.474	4425.560983(58)	4423.690
D_J	/ kHz	2.008283(40)	2.021	1.608429(49)	1.604
D_{JK}	/ kHz	-101.1809(21)	-103.4	-108.8303(15)	-113.9
D_K	/ MHz	4.1783(39)	4.132	6.19213(63)	6.452
d_1	/ kHz	-0.410926(21)	-0.412	-0.3010587(82)	-0.301
d_2	/ kHz	-0.027954(24)	-0.0239	-0.0188128(25)	-0.0154
H_J	/ mHz	5.5695(83)	5.688	4.035(13)	3.925
H_{JK}	/ Hz	-0.4629(80)	-0.4464	-0.46703(77)	-0.4788
H_{KJ}	/ Hz	-6.733(28)	-7.879	-3.690(47)	-3.192
H_K	/ kHz	3.28(39)	0.7938	1.042(46)	1.101
h_1	/ mHz	2.1716(70)	2.189	1.5502(23)	1.486
h_2	/ mHz	0.3385(63)	0.2721	0.2059(11)	0.165
h_3	/ mHz	0.1202(45)	0.0733	0.06093(23)	0.0450
L_{JK}	/ μ Hz	3.06(38)	-	-	-
L_{JK}	/ mHz	-0.3330(28)	-	-0.3403(98)	-
L_{KKJ}	/ mHz	-	-	-2.11(32)	-
χ_{aa}	/ MHz	-4.0641(61)	-4.1900	1.035(39)	0.9311
$\chi_{bb} - \chi_{cc}$	/ MHz	-2.654(15)	-2.7758	-7.6632(96)	-7.8950
σ_w		0.91		0.88	
no. of lines		531		545	

^a Equilibrium constants from extrapolated best structure, zero-point vibrational corrections computed at fc-MP2/aug-cc-pVTZ. Quartic centrifugal distortion constants computed using a composite scheme. Sextic centrifugal distortion constants computed at fc-CCSD(T)/cc-pVTZ. Nuclear quadrupole coupling constants computed at the ae-CCSD(T)/cc-pwCV5Z level. See Appendix A for further explanation.

Table 3. Rotational, hyperfine, and vibrational partition functions for PGIM isomers.

T / K	Z-PGIM			E-PGIM		
	Q_{rot}	Q_{HFS}	Q_{vib}	Q_{rot}	Q_{HFS}	Q_{vib}
3	26.073	78.218	1.0000	24.593	73.779	1.0000
5	55.562	166.69	1.0000	52.409	157.23	1.0000
10	156.05	468.14	1.0000	147.20	441.59	1.0000
15	286.02	858.06	1.0000	269.81	809.43	1.0000
25	614.37	1843.11	1.0000	579.58	1738.72	1.0000
50	1736.09	5208.26	1.0026	1637.91	4913.72	1.0022
100	4911.56	14734.7	1.0674	4634.74	13904.21	1.0637
150	9028.77	27086.3	1.2375	8520.22	25560.7	1.2301
225	16602.6	49807.8	1.7010	15634.8	46904.5	1.6883
300	25569.7	76708.8	2.5137	23925.1	71774.9	2.4962

They exactly match the CDMS² (Müller et al. 2005; Endres et al. 2016) and JPL³ (Pickett et al. 1998) file format, and are thus suited for a direct use in widespread astronomy line analysis

tools, such as CASSIS⁴ and MADCUBA (Rivilla et al. 2016). For each isomer, the results of two separate computations are provided. The files `x-pgim.cat` contain a listing of pure rotational frequencies extending up to 600 GHz, whereas the files `x-pgim_hfs.cat` provides a list of hyperfine components lim-

² <https://cdms.astro.uni-koeln.de/cdms>

³ <http://spec.jpl.nasa.gov/>

⁴ CASSIS is a software package for the analysis of astronomical spectra developed by IRAP-UPS/CNRS (<http://cassis.irap.omp.eu>).

ited to 200 GHz. The first character (x) of the file names takes the values z or e according to which isomer the file refers to. In all catalogues, the integrated intensity of each transition is computed at 300 K in order to comply with the CDMS standard.

A selection of rotational (Q_{rot}), hyperfine (Q_{HFS}), and vibrational (Q_{vib}) partition functions for PGIM isomers is provided in Table 3. The values are computed for temperatures ranging in the 3–300 K interval, and they are obtained by direct summation over the rotational or hyperfine levels whose energy position is accurately determined during the spectral analysis. The vibrational partition functions are computed through direct summation on all energy levels (including combinations and overtones), which give a contribution to Q_{vib} higher than 10^{-7} .

5. Detection of PGIM in the Galactic Center cloud G+0.693

5.1. Observations

We have searched for PGIM towards the molecular cloud G+0.693-0.027 (G+0.693 hereafter) located in the “Central Molecular Zone” (CMZ), the inner ~ 500 pc of our Galaxy. G+0.693, located at ~ 1 arcmin north-east of the star-forming protocluster SgrB2(N), does not show any sign of on-going massive star formation such as H_2O masers, H II regions or dust continuum sources (e.g., Ginsburg et al. 2018). However, despite being a quiescent cloud, it is one of the main repositories of COMs in the Galaxy (Requena-Torres et al. 2008; Zeng et al. 2018). Among the many molecules detected in this cloud, there are several species directly related with prebiotic chemistry like the simplest sugar glycolaldehyde (CH_2OHCHO ; Requena-Torres et al. 2006), formamide and methyl isocyanate (NH_2CHO and CH_3NCO , respectively; Zeng et al. 2018), phosphorous-bearing species such as PO (Rivilla et al. 2018), and recently urea (NH_2CONH_2 , Jiménez-Serra et al. 2020). In addition, several imines have been reported towards G+0.693: methanimine (CH_2NH , Zeng et al. 2018), ethanimine (CH_3CHNH , Rivilla in prep.), and the E , Z isomers of C -cyanomethanimine, NCCHNH , NCCHNH (Rivilla et al. 2019), a possible precursor of adenine, which is one of the DNA and RNA nucleobases. For Z - NCCHNH , it has been the first detection in the ISM. Therefore, G+0.693 is a promising target for the detection of new imines such as PGIM.

We have searched for PGIM in a spectral survey of G+0.693 conducted with the IRAM 30 m telescope at 3 and 2 mm. The observations were performed in two different observing runs during 2019: April 10-16 (project 172-18), and August 13-19 (project 018-19). We used the broad-band Eight MIXer Receiver (EMIR) and the fast Fourier transform spectrometers in FTS200 mode, which provided a channel width of ~ 200 kHz, i.e. a velocity resolution of ~ 0.35 – 0.85 km s^{-1} . Since we are interested in weak line emissions, we smoothed all the spectra to 5 km s^{-1} velocity resolution, enough to resolve the line widths of ~ 20 km s^{-1} measured in this source. Each spectral setup was observed several times slightly changing the central frequency (by 20–100 MHz shifts) in order to identify possible spectral features resulting from unsuppressed image side band emission.

5.2. Data analysis and results

The two intervals of frequency covered by the survey are 71.76–116.72 GHz and 124.77–175.5 GHz. During the observations, the pointing was checked every 1–1.5 h on nearby planets, QSOs or bright H II regions, and the telescope focus was checked

at the beginning of the observations and after sunset and sunrise. The half-power beam width (HPBW) of the telescope at the observed frequencies is $14''$ – $33''$. The observations were centred at the coordinates of G+0.693: $\alpha(\text{J2000}) = 17^{\text{h}}47^{\text{m}}22^{\text{s}}$ and $\delta(\text{J2000}) = -28^{\circ}21'27''$. The position switching mode was used in all the observations, with an off position of ($-885''$, $290''$). The line intensity of the spectra is given in T_{A}^* as the molecular emission towards G+0.693 is extended over the full beam (Requena-Torres et al. 2006; Martín et al. 2008; Rivilla et al. 2018). Contamination by image-band lines have been identified and eliminated during the data reduction comparing the same frequency band observed with two different spectral setups.

The identification of the molecular lines was performed using the new spectroscopic data of PGIM and the SLIM (Spectral Line Identification and Modelling) tool within the MAD-CUBA package⁵ (Martín et al. 2019). SLIM generates synthetic spectra of molecular species under the assumption of Local Thermodynamic Equilibrium (LTE) conditions. We used the MADCUBA-AUTOFIT tool that compares the observed spectra with LTE synthetic spectra, and provides the best non-linear least-squares fit using the Levenberg-Marquardt algorithm (see details in Martín et al. 2019). The free parameters of the fit are: the molecular column density (N), the excitation temperature (T_{ex}), the systemic velocity (v_{LSR}) and the full width half maximum (FWHM) of the line Gaussian profiles. Since the fit convergence was difficult to achieve when trying to optimise all four parameters, we fixed the v_{LSR} and the FWHM to 69 km s^{-1} and 20 km s^{-1} , respectively. These values allowed to reproduce well all the observed spectra and are consistent with the ones derived for other imines in the same source (Zeng et al. 2018; Rivilla et al. 2019). We have also fixed the excitation temperature to 8 K, as found for C -cyanomethanimine (Rivilla et al. 2019) as well as for other complex organic molecules (Requena-Torres et al. 2006, 2008). This value also compares well to that obtained for the simplest imine, CH_2NH , which was 9.7 ± 0.4 K (Zeng et al. 2018).

The 18 brightest transitions of Z -PGIM detected in our data at level $> 2.5\sigma$ are illustrated in Fig. 5. The resulting line parameters are summarised in Table 4. For each transition, we have evaluated the possible blending with other molecular species. We have searched in the spectral survey for more than 300 different molecules, which include all the species detected so far in the ISM⁶. The complete list of the molecular species detected in the survey will be presented in a forthcoming paper. For the scope of this work, we show in Fig. 5 the contribution of the molecules identified in the spectral intervals around the transitions assigned for Z -PGIM. Note that the low excitation temperature of the COMs detected in this source guarantees that only the lowest energy levels of these molecules are populated (see Table 4). This implies that line confusion is expected to be less severe in this source than in hot core sources such as SgrB2(N) (e.g., Belloche et al. 2019) in spite of the larger line widths. Therefore, the level of line blending of the molecular lines, especially at 3 mm, is expected to be low.

We have run AUTOFIT to derive the column density of Z -PGIM using the transitions that are less blended with other species (indicated with an asterisk in Table 4). The resulting simulated spectra are presented in red solid lines in Fig. 5. The Z -PGIM transitions have integrated intensities $\int T_{\text{A}}^* dv >$

⁵ Madrid Data Cube Analysis on ImageJ is a software developed at the Centre of Astrobiology (CAB) in Madrid; <http://cab.inta-csic.es/madcuba/Portada.html>.

⁶ <https://cdms.astro.uni-koeln.de/classic/molecules>.

Table 4. Transitions of Z-PGIM detected towards G+0.693.

Frequency ^a (GHz)	Transition	$\log I^{(b)}$ ($\text{nm}^2 \text{ MHz}$)	E_{up} (cm^{-1})	$\int T_{\text{A}}^* dv$ (mK km s^{-1})	Detection level ^c
72.898955*	8 _{1,8} – 7 _{1,7}	-4.315	10.18	281	8.0
74.355828*	8 _{0,8} – 7 _{0,7}	-4.288	8.70	378	16.4
74.537358*	8 _{2,7} – 7 _{2,6}	-4.328	15.37	107	4.2
74.742197*	8 _{2,6} – 7 _{2,5}	-4.325	15.38	107	4.6
76.127838	8 _{1,7} – 7 _{1,6}	-4.278	10.56	271	9.9
81.995559*	9 _{1,9} – 8 _{1,8}	-4.166	12.61	222	8.0
83.587572	9 _{0,9} – 8 _{0,8}	-4.141	11.18	295	13.5
83.842907*	9 _{2,8} – 8 _{2,7}	-4.174	17.86	84	4.3
84.134809	9 _{2,7} – 8 _{2,6}	-4.171	17.87	84	4.1
85.625901*	9 _{1,8} – 8 _{1,7}	-4.129	13.10	209	5.4
91.086864*	10 _{1,10} – 9 _{1,9}	-4.034	15.35	162	10.1
92.797807*	10 _{0,10} – 9 _{0,9}	-4.010	13.96	212	14.1
95.117382*	10 _{1,9} – 9 _{1,8}	-3.997	15.95	149	7.0
100.172426*	11 _{1,11} – 10 _{1,10}	-3.916	18.39	109	3.0
101.984662	11 _{0,11} – 10 _{0,10}	-3.894	17.06	141	4.7
104.601405*	11 _{1,10} – 10 _{1,9}	-3.880	19.13	98	3.0
109.251842	12 _{1,12} – 11 _{1,11}	-3.809	21.73	68	3.2
111.146539	12 _{0,12} – 11 _{0,11}	-3.789	20.46	87	2.7

^a Asterisks denote the transitions used in the MADCUBA–AUTOFIT analysis.

^b base 10 logarithm of the integrated intensity of the transition at 300 K.

^c See text of Sect. 5.2.

68 mK km s⁻¹ (see Table 4). We calculated the detection level of each transition by comparing the velocity-integrated intensity with $\sigma = \text{rms} \times \sqrt{\delta v / \text{FWHM}} \times \text{FWHM}$, where rms is the noise root-mean-square measured over a line-free spectral range of $\pm 500 \text{ km s}^{-1}$ around each transition, and δv is the spectral resolution expressed in velocity units. The derived rms are in the range 1.5–3.9 mK km s⁻¹ in channels of 5 km s⁻¹. As indicated in Table 4, 14 transitions are detected above 4σ , and 8 transitions are above 6σ . The integrated intensities corresponding to the fitted column densities derived by AUTOFIT are shown in Table 5. The column density of Z-PGIM is $(0.24 \pm 0.02) \times 10^{14} \text{ cm}^{-2}$. By considering the H₂ column density towards G+0.693, $N_{\text{H}_2} = 1.35 \times 10^{23} \text{ cm}^{-2}$ (Martín et al. 2008), we can derive a Z-PGIM fractional abundance of 1.8×10^{-10} .

The higher-energy E-PGIM isomer is not detected in the data. To derive its upper limit we have used the two brightest spectral features that appear completely free of contamination by other species in the observed spectra: the hyperfine $\Delta F = +1$ triplet of the $J_{K_a, K_c} = 5_{1,5} - 4_{0,4}$ line centred at 101 915 MHz ($E_L = 3.07 \text{ cm}^{-1}$), and the one of the $J_{K_a, K_c} = 6_{1,6} - 5_{0,5}$ line at 110 103 GHz ($E_L = 4.60 \text{ cm}^{-1}$). We adopted the same assumptions on excitation temperature, velocity and line FWHM as for the Z-PGIM. The upper limits to the integrated intensity are derived using the formula $3 \times \text{rms} \times \Delta v / \sqrt{n_{\text{chan}}}$, where n_{chan} is the number of channels covered by the full line width Δv . The upper limit derived for the column density of E-PGIM is $N < 1.3 \times 10^{13} \text{ cm}^{-2}$. This implies an isomer abundance ratio of $[Z]/[E] > 1.9$, hinting at a higher abundance of the thermodynamically more stable form.

We also report fractional abundances of other molecular species that might be chemically related to PGIM: cyanoacetylene (HC₃N), acrylonitrile (CH₂CHCN), propyne (CH₃CCH), C-cyanomethanimine (NCCHNH), ethynyl (CCH), and propynal (HCCCHO). All of them are detected towards G+0.693 and have abundances $\geq 10^{-9}$. The derived parameters are presented in Table 5. For CH₃CCH, we have fitted the $J = 9 - 8, 8 - 7, 6 - 5$ and $5 - 4$ transitions with $K = 0, 1$. For CCH, we derived its abundance by fitting the optically thin lines of the isotopic variant C¹³CH, and assuming the isotopic ratio of ¹²C/¹³C ~ 21 measured in G+0.693 by Armijos-Abendaño et al. (2015). For HC₃N, CH₂CHCN, and NCCHNH, we adopted the values obtained in previous works (Zeng et al. 2018; Rivilla et al. 2019), whereas the HCCCHO results are taken from a full chemical analysis of the source that will be presented in a forthcoming paper (Rivilla in prep.).

5.3. Discussion

To the best of our knowledge, the formation of PGIM in the ISM has never been investigated to date, thus there are no chemical pathways included in astrochemical databases such as KIDA⁷ (Wakelam et al. 2012) or UMIST⁸ (McElroy et al. 2013). In the following, we formulate and discuss a few possible PGIM formation mechanism based on the results of theoretical and experimental studies on detected imines (e.g. Lovas et al. 2006; Theule et al. 2011; Krim et al. 2019):

⁷ <http://kida.obs.u-bordeaux1.fr>.

⁸ <http://udfa.a.jmarkwick.net/index.php>.

Table 5. Derived physical parameters for PGIM isomers and proposed molecular precursors.

Molecule	N (10^{14} cm^{-2})	T_{ex} (K)	v_{LSR} (km s^{-1})	FWHM (km s^{-1})	Abundance ^a ($\times 10^{-10}$)	Reference ^b
Z-PGIM	0.24 ± 0.02	8	69	20	1.8	1
E-PGIM	< 0.13	8	69	20	< 0.9	1
CH ₃ CCH ^c	17.0 ± 2	19 ± 1	69	20	126	1
HC ₃ N ^d	7.1 ± 1.3	12 ± 2	68 ± 1	22 ± 1	53	2
CH ₂ CHCN	0.9 ± 0.1	10.8 ± 1.1	68 ± 1	22 ± 2	7	2
CCH ^d	53 ± 7	–	–	–	391	1
Z-NCCHNH	2.0 ± 0.6	8 ± 2	68.3 ± 0.8	20	15	3
E-NCCHNH	0.33 ± 0.03	8	68.0 ± 0.8	21 ± 2	2.4	3
HCCCHO	0.32 ± 0.02	18 ± 2	67.6 ± 0.4	20	2.4	4

^a We adopted $N_{\text{H}_2} = 1.35 \times 10^{23} \text{ cm}^{-2}$ as inferred by Martín et al. (2008) from C¹⁸O observations.

^b References: (1) This work; (2) Zeng et al. (2018); (3) Rivilla et al. (2019); (4) Rivilla (in prep.).

^c Fit obtained from the $J = 9 - 8, 8 - 7, 6 - 5$ and $5 - 4$ transitions with $K = 0$ and $K = 1$.

^d The column densities of HC₃N and CCH were derived from the optically thin transitions of the H¹³CCCN and C¹³CH isotopologues, respectively. The isotopic ratio of ¹²C/¹³C ~ 21 measured by Armijos-Abendaño et al. (2015) in G+0.693 was used.

- (a) hydrogenation of cyanoacetylene (possibly on dust grains);
- (b) tautomerisation of acrylonitrile;
- (c) neutral–neutral reaction between *C*-cyanomethanimine and the ethynyl radical to form PGIM and the CN radical;
- (d) reaction of propynal and ammonia followed by water elimination;
- (e) hydrogen abstraction on propyne which gives PGIM after reaction with the imidogen radical.

The schematic reactions are illustrated in Fig. 6. As shown in Table 5, all the proposed processes involve molecular precursors that are significantly more abundant than PGIM (although propynal only marginally), therefore it is not unlikely that one (or several) of these mechanisms might be able to account for the presence of this imine in G+0.693.

The route (a) involves selective hydrogenation of the C \equiv N group on dust grain surfaces. This process has proved to be effective for generating fully saturated methylamine from HCN ices (Theule et al. 2011), although the intermediate imine was not observed. More doubtful is the viability of this chemical scheme starting from larger nitriles. For example, the formation of ethanimine from CH₃CN, as suggested by Loomis et al. (2013), seems to be unlikely in view of recent laboratory works (Nguyen et al. 2019), which investigated the co-deposition of methyl cyanide and H atoms and showed that the C \equiv N moiety is not reduced in the 10–60 K temperature range. In the absence of energetic processes, the hydrogenation of cyanoacetylene would result in a competition of the H attack to the C \equiv C and C \equiv N triple bonds, leading mainly to acrylonitrile (Krim et al. 2019, route a’). However, route (a) cannot be completely ruled out as the chemistry in G+0.693 is known to be shock-dominated (e.g., Rivilla et al. 2019). Also, cosmic-ray ionisation rate is expected to be high across the Galactic Centre (Goto et al. 2013) and also likely high in G+0.693 (see Zeng et al. 2018), thus providing an additional source of energy.

Route (b) is analogous to the proposed CH₃CN \rightarrow CH₂=C=NH conversion driven by shocks (Lovas et al. 2006). The energetics of the Z-PGIM \rightarrow CH₂=CHCN

tautomerisation has been investigated theoretically by Osman et al. (2014). Their calculations (at the MP2 level of theory) show that acrylonitrile is more stable than Z-PGIM by 32.7 kcal mol⁻¹ ($E/k \approx 16\,500$ K), and the double H migration involved in the process has barrier energies exceeding 80 kcal mol⁻¹ ($E/k \approx 40\,300$ K). They concluded that CH₂=CHCN is dominant in the cold ISM, and point to a conversion to PGIM possibly occurring in shock-dominated regions or hot cores. The above figures however, seems to be too high to allow for such a pathway in the shocks affecting G+0.693 (Requena-Torres et al. 2006).

Route (c), (d), and (e), require two molecules to be co-spatial. In all these processes, at least one reactant is much more abundant than PGIM in G+0.693: (ethynyl, propyne, and ammonia), hence they are feasible in principle. Route (d) seems to be less likely because propynal is only marginally more abundant than PGIM, unlike the other two reactants, *C*-cyanomethanimine and propyne, which are factors of ~ 10 and ~ 100 more abundant, respectively. However, given the lack of information on the associated reaction rates and energy barriers, only speculative reasoning can be done.

In analogous cases, hints to constrain the formation scenario can be provided by the observed $[Z]/[E]$ isomer abundance ratio. It has been proposed that the relative abundances of structural isomers in the ISM might be established by their thermodynamic stabilities (minimum energy principle, see Lattelais et al. 2009). Although there are some well known exceptions (H₄C₂O₂ and H₂C₃O isomers; see also Shingledecker et al. 2019), this hypothesis seems to work well, at least for simple cases of geometrical isomerism. Rivilla et al. (2019), for example, showed that the ratio between the *Z*- and *E*- isomers of *C*-cyanomethanimine (NCCHNH) does follow thermodynamic equilibrium:

$$[Z]/[E] = \frac{N(Z)}{N(E)} = \frac{1}{g} \exp\left(\frac{\Delta E}{T_k}\right), \quad (3)$$

where ΔE is the energy difference between the two isomers, T_k is the kinetic temperature of the gas, and g is a factor that

accounts for statistical weights (1 for the *Z*- and *E*- isomers of both NCCHNH and PGIM). The $[Z]/[E] \sim 6$ found for *C*-cyanomethanimine, implies a T_k in the 130–210 K range, which is in good agreement with the kinetic temperature measured by Zeng et al. (2018) in G+0.693⁹.

According to our newly performed ab initio calculations (see Appendix A), the $\Delta E/k$ for PGIM isomers is 428.2 K. Using this value, the $[Z]/[E]$ ratio expected for PGIM for the T_k range 130–210 K, is 8–27. This prediction is consistent with the observed lower limit of $[Z]/[E] > 1.9$, but the lack of a more stringent upper limit for *E*-PGIM prevents a firm confirmation that PGIM isomers actually follow the relative abundance predicted by thermodynamics.

The cosmic-ray ionization rate in the CMZ where G+0.693 is located is expected to be factors of 10–100 higher in the Galactic centre than in the disc, as measured by Goto et al. (2013, 2014) using H_3^+ observations. Zeng et al. (2018) suggested that a relatively high cosmic-ray ionisation rate of $1 - 10 \times 10^{-15} \text{ s}^{-1}$ might be responsible of the cyanopolynes and nitriles molecular ratios found in G+0.693. Indeed, this produce an enhanced abundance of C atoms, due to the efficient CO destruction (Bisbas et al. 2019), possibly accounting for the large abundance of carbon-chains in this region. Also, a high cosmic-ray ionisation rate can create atomic hydrogen (H) in an efficient way from the dissociation of H_2 (Padovani et al. 2018); then, different reactivity of the PGIM isomers with atomic H might produce the different abundances observed. However, theoretical quantum chemical calculations of the reactions of PGIM isomers with H need to be performed to test this possibility.

Another possible destruction route is through charged species such as H_3^+ . In this case, the destruction rates depend on the permanent dipole moment of the different isomers. For *C*-cyanomethanimine, the *E* isomer presents a dipole moment that is a factor of ~ 3 higher than the one of the *Z* isomer. Shingledecker (submitted) has shown theoretically that this produces a more efficient destruction of the *E* by reaction with H_3^+ , which may contribute to its lower abundance observed in G+0.693. This explanation, however, cannot be applied to PGIM, since both *Z* and *E* isomers have very similar modulus of their permanent dipole moments (see Section 3). Therefore, one should expect similar destruction rates for both isomers with H_3^+ .

6. Conclusions

This paper presents an extensive theoretical and laboratory study of the rotational spectrum of PGIM in its vibrational ground state, extending the earlier, very limited knowledge on the spectroscopic properties of this simple imine. The recordings have been performed in selected frequency intervals spanning the 83–500 GHz range, collecting some 500 lines for each of the two *E* and *Z* geometrical isomers. These experimental data were fitted to the coefficients of the *S*-reduced rotational Hamiltonian, providing a very precise set of rotational, quartic, and sextic centrifugal distortion constants. Many transitions, especially those of *b*-type dipole, show a resolvable hyperfine patterns due to the quadrupole coupling of the ^{14}N nuclei. For these transitions, 357 separate components were accurately measured and analysed to determine the corresponding hyperfine coupling coefficients. The optimised values of all the spectroscopic con-

stants are in excellent agreement with the results of high-level theoretical calculations, which were performed to assist the analysis of the laboratory data.

The newly obtained set of spectroscopic parameters (Tables 2) allowed to generate a highly precise set of rest-frequencies for *E*- and *Z*-PGIM at mm regime. With these data we have searched for PGIM in a spectral survey of the molecular cloud G+0.693 located in the “Central Molecular Zone”. We have detected 18 transitions of *Z*-PGIM, the lowest energy isomer, for which a column density of $N = (0.24 \pm 0.02) \times 10^{14} \text{ cm}^{-2}$ was derived. The higher-energy *E*-PGIM isomer was not detected in the data, setting an upper limit of $N < 1.3 \times 10^{13} \text{ cm}^{-2}$ from the two strong spectral features which show no contamination from other species.

The fractional abundance (w.r.t. H_2) derived for *Z*-PGIM is 1.8×10^{-10} . This value was compared with the ones found for possible chemical precursors, i.e., cyanoacetylene (HC_3N), propyne (CH_3CCH), acrylonitrile (CH_2CHCN), *C*-cyanomethanimine (NCCHNH), ethynyl (CCH), and propynal (HCCCHO). The relative abundance of all of them detected towards G+0.693 are higher (by up to two orders of magnitude for CH_3CCH) than that of PGIM.

Acknowledgements. We thank the IRAM-30m staff for the precious help during the different observing runs. A.P.C. gratefully acknowledges financial support by University Cà Foscari Venezia (AdiR funds) and the super-computing facilities of CINECA (project “CINEMA”, grant HP10C2QE6F) and SCSCF (“Sistema per il Calcolo Scientifico di Cà Foscari”, a multiprocessor cluster system owned by Università Cà Foscari Venezia). V.M.R. has received funding from the European Union’s Horizon 2020 research and innovation programme under the Marie Skłodowska-Curie grant agreement No 664931. I.J.-S. and J.M.-P. have received partial support from the Spanish FEDER (project number ESP2017-86582-C4-1-R), and State Research Agency (AEI) through project number MDM-2017-0737 Unidad de Excelencia María de Maeztu–Centro de Astrobiología (INTA-CSIC). J.C.G. thanks the program Physique et Chimie du Milieu Interstellaire (INSU-CNRS), the Centre National d’Etudes Spatiales (CNES) and the PHC Procope 42516WC (CAMPUS France) for financial support. D.P. and L.B. and acknowledge DAAD support through the project 57445281 “Small organic molecules in the Interstellar Medium” in the framework of “Programm Projektbezogener Personenaustausch Frankreich (Phase I) 2019”. S.Z. acknowledges support from RIKEN Special Postdoctoral Researcher Program.

⁹ The T_k value found for G+0693 is significantly lower than the average T_{ex} of the observed molecules (see Table 5) as, due to the low density of the source, their rotational energy level manifolds are sub-thermally populated.

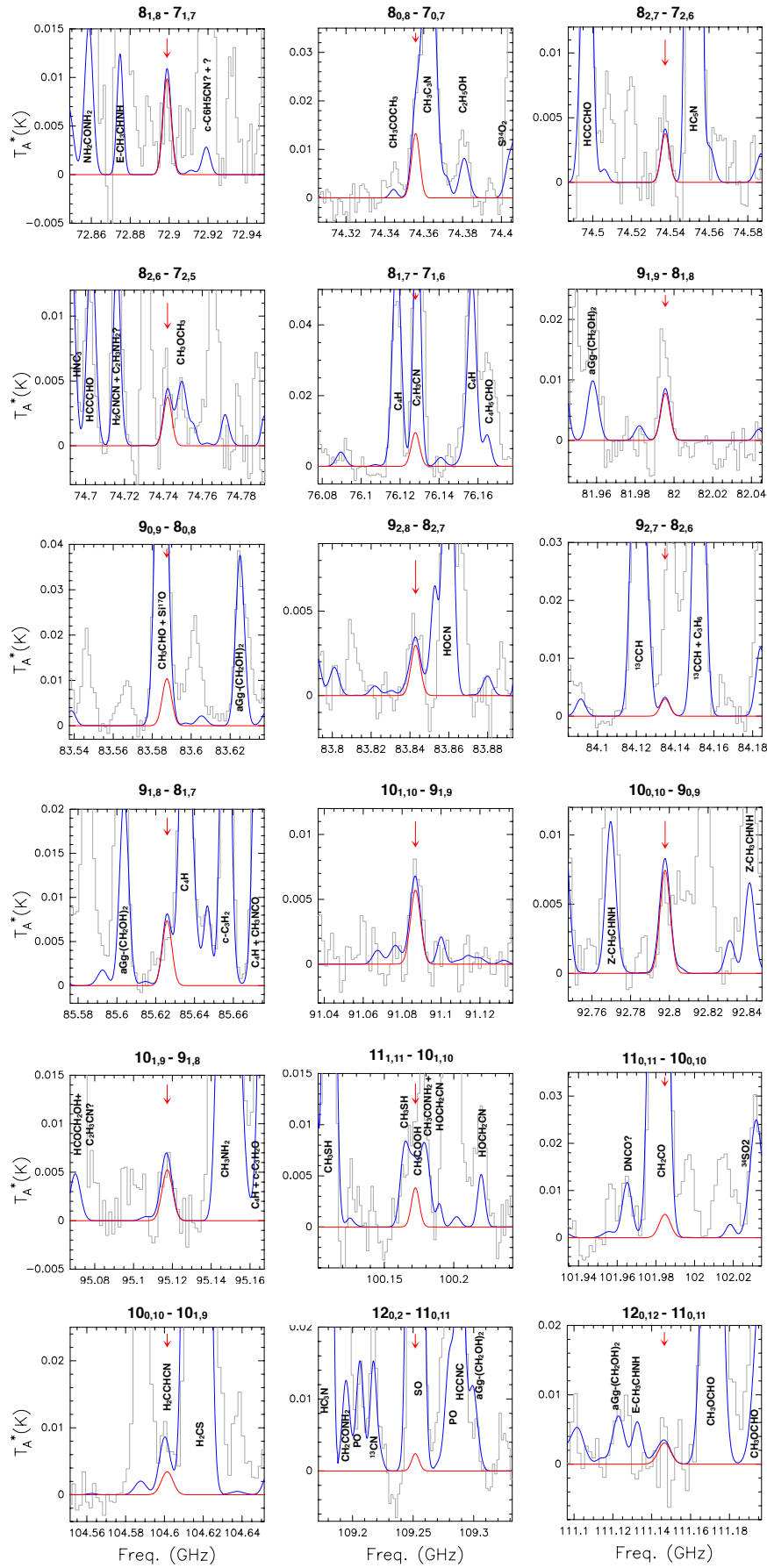


Fig. 5. LTE spectrum (in red) of the 18 brightest transitions of Z-PGIM detected towards G+0.693. The contribution of all the species identified in the source so far is indicated with a blue curve.

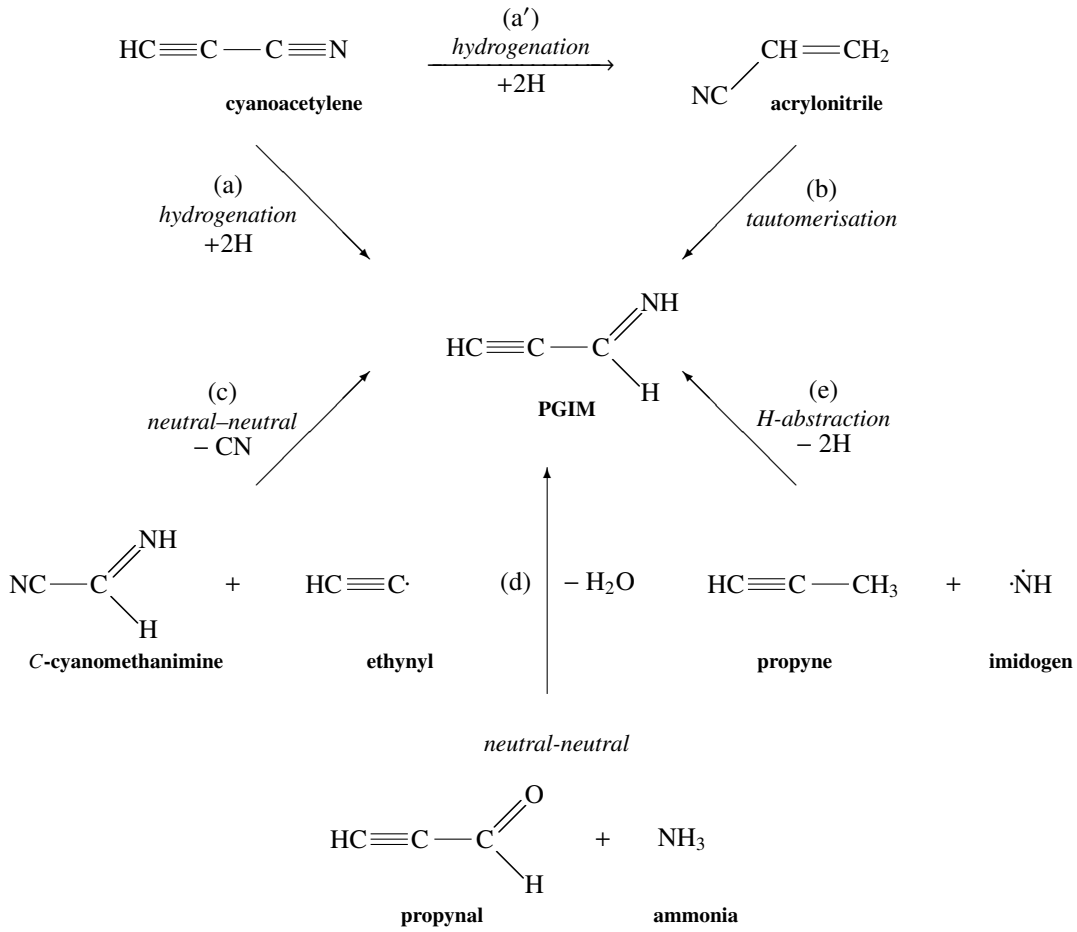


Fig. 6. Possible formation mechanisms of PGIM in the ISM.

Appendix A: Details of the theoretical calculations

For calculating the equilibrium structures, extrapolation to the complete basis set (CBS) limit was performed for both the Hartree-Fock self-consistent-field (HF-SCF) and the valence correlation (evaluated at the frozen-core (fc) CCSD(T) level of theory) terms, using the formulas of Halkier et al. (1999) for the former and the two-parameter correction of Helgaker et al. (1997b) for the latter. At HF-SCF level of theory, the correlation consistent polarised basis sets $cc\text{-}pVnZ$ ($n = T, Q, 5$) of Dunning (1989) and Woon & Dunning (1995) were used, while the fc-CCSD(T) calculations were carried out by using the $cc\text{-}pVTZ$ and $cc\text{-}pVQZ$ basis sets. For computing the contribution related to the core-valence (CV) electron correlation the difference between the all-electron (ae) and frozen-core results using the $cc\text{-}pCVTZ$ basis set (Woon & Dunning 1995) was used, while the contribution due to the diffuse functions was calculated by employing the $aug\text{-}cc\text{-}pVTZ$ basis set (Kendall et al. 1992). All these terms were evaluated at CCSD(T) level of theory. The energies of these two structures were computed with the same approach but using the $cc\text{-}pVnZ$ ($n = Q, 5, 6$) basis sets. The vibrational corrections to both the equilibrium rotational constants were calculated at fc-MP2 level of theory (Møller & Plesset 1934) and using the $aug\text{-}cc\text{-}pVTZ$ basis set; the same level of theory provided also the anharmonic corrections used to compute the fundamental frequencies reported in Table A.2. The cubic force field data needed for determining the sextic centrifugal distortion constants were obtained at CCSD(T) level on the basis of its good accuracy reported in the literature (Pietropolli Charmet et al. 2017b). Nuclear quadrupole coupling constants for the nitrogen atoms were computed at ae-CCSD(T) level of theory in conjunction with the $pw\text{-}CV5Z$ basis set (Dunning 1989; Peterson & Dunning 2002) following the same procedure described previously (Cazzoli et al. 2011; Pietropolli Charmet et al. 2016).

All the calculations carried out at CCSD(T) and MP2 level of theory were performed by using the CFOUR¹⁰ suite of programs and its implementation of analytic second derivatives (Gauß & Stanton 1997), while the sextic centrifugal distortion constants were computed using an appropriate suite of programs (Pietropolli Charmet & Cornaton 2018) and the formulas reported in the literature (Aliev & Watson 1976; Watson 1977; Aliev & Watson 1985).

A summary of the results provided by the present ab initio calculations is presented in Table A.1 together with the comparison with the values reported in the literature (Sugie et al. 1985; Osman et al. 2014).

Concerning the equilibrium molecular parameters obtained by our calculations, on the basis of previous studies (see, for example Bak et al. 2001), we may estimate an overall accuracy of $2\text{--}3 \times 10^{-3}$ Å for bond distances. For comparison, the bond lengths reported by Sugie et al. (1985) listed in Table A.1 are generally shorter, while the ones computed by Osman et al. (2014) (listed in the same Table) are generally longer. These discrepancies are due to the low level of theory used in these earlier studies. As a matter of fact, the accuracy of molecular equilibrium structures is strongly dependent on the wave func-

tion method employed; for example, it is reported that computations carried out at HF level of theory generally underestimate the bond lengths, while CCSD calculations, depending on the basis set used, may predict values that are either too short or too long (Helgaker et al. 1997a).

As an independent test of the overall reliability of the theoretical calculations, one can apply the ab initio zero-point vibrational contributions to the experimentally derived ground state rotational constants and obtain the so-called “semi-experimental” equilibrium rotational constants. From these quantities the inertial defect can be estimated yielding $-6.7 \times 10^{-4} \text{ u Å}^2$ for Z-PGIM and $-2.7 \times 10^{-3} \text{ u Å}^2$ for E-PGIM. These values are very close to zero as expected for a molecule with planar equilibrium configuration, thus indicating that both the electronic structures and the vibrational dynamics have been correctly modelled (McCarthy et al. 2016).

References

- Aliev, M. R. & Watson, J. K. G. 1976, *J. Mol. Spectrosc.*, 61, 29
- Aliev, M. R. & Watson, J. K. G. 1985, in *Molecular Spectroscopy: Modern Research*, ed. K. N. Rao, Vol. III (Academic Press, New York), 1–67
- Altwegg, K., Balsiger, H., Bar-Nun, A., et al. 2016, *Sci. Adv.*, 2, e1600285
- Aponte, J. C., Elsila, J. E., Glavin, D. P., et al. 2017, *ACS Earth and Space Chemistry*, 1, 3
- Armijos-Abendaño, J., Martín-Pintado, J., Requena-Torres, M. A., Martín, S., & Rodríguez-Franco, A. 2015, *MNRAS*, 446, 3842
- Bak, K. L., Gauss, J., Jørgensen, P., et al. 2001, *J. Chem. Phys.*, 114, 6548
- Barone, V., Biczysko, M., & Puzzarini, C. 2015, *Acc. Chem. Res.*, 48, 1413
- Belloche, A., Garrod, R. T., Müller, H. S. P., et al. 2019, *A&A*, 628, A10
- Bisbas, T. G., Schrubba, A., & van Dishoeck, E. F. 2019, *MNRAS*, 485, 3097
- Bizzocchi, L., Lattanzi, V., Laas, J., et al. 2017a, *A&A*, 602, A34
- Bizzocchi, L., Tamassia, F., Laas, J., et al. 2017b, *ApJS*, 233, 11
- Burton, A. S., Stern, J. C., Elsila, J. E., Glavin, D. P., & Dworkin, J. P. 2012, *Chem. Soc. Rev.*, 41, 5459
- Cazzoli, G., Cludi, L., Puzzarini, C., et al. 2011, *J. Phys. Chem. A*, 115, 453
- Cobb, A. K. & Pudritz, R. E. 2014, *ApJ*, 783, 140
- Danger, G., Borget, F., Chomat, M., et al. 2011a, *A&A*, 535, A47
- Danger, G., Bossa, J. B., de Marcellus, P., et al. 2011b, *A&A*, 525, A30
- Degli Esposti, C., Dore, L., Puzzarini, C., et al. 2018, *A&A*, 615, A176
- Dickens, J. E., Irvine, W. M., De Vries, C. H., & Ohishi, M. 1997, *ApJ*, 479, 307
- Dunning, Jr., T. H. 1989, *J. Chem. Phys.*, 90, 1007
- Endres, C. P., Schlemmer, S., Schilke, P., Stutzki, J., & Müller, H. S. P. 2016, *J. Mol. Spectrosc.*, 327, 95
- Gambi, A., Pietropolli Charmet, A., Stoppa, P., et al. 2019, *Phys. Chem. Chem. Phys.*, 21, 3615
- Gardner, F. F. & Winniewisser, G. 1970, *ApJ*, 195, L127
- Gauß, J. & Stanton, J. F. 1997, *Chem. Phys. Lett.*, 276, 70
- Ginsburg, A., Bally, J., Barnes, A., et al. 2018, *ApJ*, 853, 171
- Godfrey, P. D., Brown, R. D., Robinson, B. J., & Sinclair, M. W. 1973, *ApL*, 13, 119
- Gordy, W. & Cook, R. L. 1984, *Microwave molecular spectra* (Wiley, New York)
- Goto, M., Geballe, T. R., Indriolo, N., et al. 2014, *ApJ*, 786, 96
- Goto, M., Indriolo, N., Geballe, T. R., & Usuda, T. 2013, *J. Phys. Chem. A*, 117, 9919
- Halkier, A., Helgaker, T., Jørgensen, P., Klopper, W., & Olsen, J. 1999, *Chem. Phys. Lett.*, 302, 437
- Hamada, Y., Tsuboi, M., Takeo, H., & Matsumura, C. 1984, *J. Mol. Spectrosc.*, 106, 175
- Heckert, M., Kállay, M., & Gauss, J. 2005a, *Mol. Phys.*, 103, 2109
- Heckert, M., Kállay, M., Tew, D. P., Klopper, W., & Gauss, J. 2005b, *J. Chem. Phys.*, 125, 044108
- Helgaker, T., Gauss, J., Jørgensen, P., & Olsen, J. 1997a, *J. Chem. Phys.*, 106, 9430
- Helgaker, T., Klopper, W., Koch, H., & Noga, J. 1997b, *J. Chem. Phys.*, 106, 9639
- Herbst, E. & van Dishoeck, E. F. 2009, *ARA&A*, 47, 427
- Jiménez-Serra, I., Martín-Pintado, J., Zeng, S., et al. 2020, in press
- Kawaguchi, K., Takano, S., Ohishi, M., et al. 1992, *ApJ*, 396, L49
- Kendall, R. A., Dunning, T. H., & Harrison, R. J. 1992, *J. Chem. Phys.*, 96, 6796
- Koch, D. M., Toubin, C., Peslherbe, G. H., & Hynes, J. T. 2008, *J. Phys. Chem. C*, 112, 2972
- Krim, L., Guillemin, J.-C., & Woon, D. E. 2019, *MNRAS*, 485, 5210
- Kroto, H. W., McNaughton, D., & Osman, I. O. 1984, *J. Chem. Soc. Chem. Comm.*, 993

¹⁰ CFOUR, Coupled-Cluster techniques for Computational Chemistry, a quantum-chemical program package written by J.F. Stanton, J. Gauss, L. Cheng, M.E. Harding, D.A. Matthews, P.G. Szalay et al., and the integral packages MOLECULE (J. Almlöf and P.R. Taylor), PROPS (P.R. Taylor), ABACUS (T. Helgaker, H.J. Aa. Jensen, P. Jørgensen, and J. Olsen), and ECP routines by A. V. Mitin and C. van Wüllen. For the current version, see <http://www.cfour.de>.

Table A.1. Theoretically computed equilibrium geometries^a, dipole moments^b, relative energy^c, and equilibrium rotational constants^c of PGIM isomers and comparison with previous works.

		Z-PGIM			E-PGIM		
		this work	Ref. (1) ^d	Ref. (2) ^e	this work	Ref. (1) ^d	Ref. (2) ^e
C≡C	/Å	1.2074	1.1845	1.226	1.2066	1.1838	1.225
C–C	/Å	1.4374	1.4480	1.460	1.4345	1.4444	1.457
C=N	/Å	1.2767	1.2504	1.288	1.2770	1.2506	1.289
H–C	/Å	1.0635	1.0558	1.076	1.0634	1.0557	1.076
C–H	/Å	1.0863	1.0780	1.100	1.0903	1.0827	1.102
N–H	/Å	1.0199	1.0060	1.029	1.0184	1.0046	1.028
∠(C–C–H)	/ deg	116.52	115.82		115.54	114.60	
∠(H–C=N)	/ deg	118.11	118.38		123.32	123.98	
∠(H–N=C)	/ deg	110.49	111.97	109.75	109.92	110.94	109.06
∠(C–C=N)	/ deg	125.37	125.80	126.68	121.14	121.42	121.00
μ_a	/ D	2.1449	2.39		0.2567	0.23	
μ_b	/ D	0.1674	0.26		1.9346	2.13	
E_0	/ kcal mol ⁻¹	0.0	0.0	0.0	0.8510	1.037	0.697
A_e	/ MHz	54525.6766	56884.0		63330.757	65775.0	
B_e	/ MHz	4876.6255	4924.0		4772.651	4833.0	
C_e	/ MHz	4476.2794	4531.0		4438.187	4502.0	

^a Extrapolated “best value”, CCSD(T)/CBS+CV.^b Extrapolated, CCSD(T)/CBS+CV (absolute values).^c See Appendix A for explanation.^d Ref. (1) is Sugie et al. (1985), computed at HF/4-31G* level of theory.^e Ref. (2) is Osman et al. (2014), computed at CCSD/aug-cc-pVDZ level of theory.**Table A.2.** Anharmonic frequencies (cm⁻¹) for the singly-excited vibrational levels of PGIM isomers^a.

level	symmetry	Z-PGIM	E-PGIM
ν_1	A'	3322	3337
ν_2	A'	3275	3286
ν_3	A'	3028	2911
ν_4	A'	2113	2121
ν_5	A'	1592	1605
ν_6	A'	1395	1385
ν_7	A'	1224	1224
ν_8	A'	922	916
ν_9	A'	640	643
ν_{10}	A'	591	596
ν_{11}	A'	211	219
ν_{12}	A''	1099	1074
ν_{13}	A''	817	795
ν_{14}	A''	646	651
ν_{15}	A''	289	285

^a Harmonic force field data corrected by cubic and quartic semi-diagonal force constants obtained by fc-MP2 calculations (see text for details).

Lattelais, M., Pauzat, F., Ellinger, Y., & Ceccarelli, C. 2009, ApJL, 696, L133
Loomis, R. A., Zaleski, D. P., Steber, A. L., et al. 2013, ApJ, 765, L9
Lovas, F. J., Hollis, J. M., Remijan, A. J., & Jewell, P. R. 2006, ApJ, 645, L137
Martín, S., Martín-Pintado, J., Blanco-Sánchez, C., et al. 2019, A&A, 631, A159
Martín, S., Requena-Torres, M. A., Martín-Pintado, J., & Mauersberger, R. 2008, ApJ, 678, 245
McCarthy, M. C., Martínez, O., McGuire, B. A., et al. 2016, J. Chem. Phys., 144, 124304
McElroy, D., Walsh, C., Markwick, A. J., et al. 2013, A&A, 550, A36
McGuire, B. A., Loomis, R. A., Charness, C. M., et al. 2012, ApJ, 758, L33

McNaughton, D., Osman, O. I., & Kroto, H. W. 1988, J. Mol. Struct., 190, 195
Møller, C. & Plesset, M. S. 1934, Phys. Rev., 46, 618
Müller, H. S. P., Schlöder, F., Stutzki, J., & Winnewisser, G. 2005, J. Mol. Struct., 742, 215
Nguyen, T., Fourré, I., Favre, C., et al. 2019, A&A, 628, A15
Osman, I. O., McNaughton, D., Suffolk, R. J., & Watts, J. D. Kroto, H. W. 1987, J. Chem. Soc. Perkin Trans. II, 683
Osman, O. I., Elroby, S. A., Aziz, S. G., & Hilal, R. H. 2014, Int. J. Mol. Sciences, 15, 11064
Padovani, M., Galli, D., Ivlev, A. V., Caselli, P., & Ferrara, A. 2018, A&A, 619, A144
Peterson, K. A. & Dunning, T. H. 2002, J. Chem. Phys., 117, 10548
Pickett, H. M. 1991, J. Mol. Spectrosc., 148, 371
Pickett, H. M., Poynter, R. L., Cohen, E. A., et al. 1998, J. Quant. Spectrosc. Radiat. Transfer, 60, 883
Pietropoli Charmet, A. & Cornaton, Y. 2018, J. Mol. Struct., 1160, 455
Pietropoli Charmet, A., Stoppa, P., Giorgianni, S., et al. 2017a, J. Phys. Chem. A, 121, 3305
Pietropoli Charmet, A., Stoppa, P., Tasinato, N., et al. 2010, J. Chem. Phys., 133, 044310
Pietropoli Charmet, A., Stoppa, P., Tasinato, N., & Giorgianni, S. 2017b, J. Mol. Spectrosc., 335, 117
Pietropoli Charmet, A., Stoppa, P., Tasinato, N., Giorgianni, S., & Gambi, A. 2016, J. Phys. Chem. A, 120, 8369
Puzzarini, C., Biczysko, M., Bloino, J., & Barone, V. 2014, ApJ, 785, 107
Raghavachari, K., Trucks, G. W., Pople, J. A., & Head-Gordon, M. 1989, Chem. Phys. Lett., 157, 479
Ramabhadran, R. O. & Raghavachari, K. 2013, J. Chem. Theor. Comp., 9, 3986
Requena-Torres, M. A., Martín-Pintado, J., Martín, S., & Morris, M. R. 2008, ApJ, 672, 352
Requena-Torres, M. A., Martín-Pintado, J., Rodríguez-Franco, A., et al. 2006, A&A, 455, 971
Rivilla, V. M., Fontani, F., Beltrán, M. T., et al. 2016, ApJ, 862, 161
Rivilla, V. M., Jiménez-Serra, I., Zeng, S., et al. 2018, MNRAS, 475, L30
Rivilla, V. M., Martín-Pintado, J., Jiménez-Serra, I., et al. 2019, MNRAS, 483, L114
Rivilla, V. M., et al., in prep.
Shingledecker, C. N., Álvarez-Barcia, S., Korn, V. H., & Kästner, J. 2019, ApJ, 878, 80
Shingledecker, C. N., et al., submitted

- Snyder, L. E., Lovas, F. J., Hollis, J. M., et al. 2005, *ApJ*, 619, 914
Sugie, M., Takeo, H., & Matsumura, C. 1985, *J. Mol. Spectrosc.*, 111, 83
Theule, P., Borget, F., Mispelaer, F., et al. 2011, *A&A*, 534, A64
Wakelam, V., Herbst, E., Loison, J.-C., et al. 2012, *ApJS*, 199, 21
Watson, J. K. G. 1967, *J. Chem. Phys.*, 46, 1935
Watson, J. K. G. 1977, in *Vibrational Spectra and Structure*, ed. J. Durig, Vol. 6 (Elsevier, Amsterdam), 1–89
Watson, J. K. G. 1977, *J. Mol. Spectrosc.*, 65, 123
Woon, D. E. 2002, *ApJ*, 571, L177
Woon, D. E. & Dunning, T. H. 1995, *J. Chem. Phys.*, 103, 4572
Zaleski, D. P., Seifert, N. A., Steber, A. L., et al. 2013, *ApJ*, 765, L10
Zeng, S., Jiménez-Serra, I., Rivilla, V. M., et al. 2018, *MNRAS*, 478, 2962